Hysteretic Faraday waves

Nicolas Périnet* and Claudio Falcón
Departamento de Física, Facultad de Ciencias Físicas y Matemáticas, Universidad de Chile, Casilla 487-3, Santiago, Chile

Jalel Chergui and Damir Juric
LIMSI, CNRS, Université Paris-Saclay, Bât 508, rue John von Neumann, Campus Universitaire, F-91405, Orsay

Seungwon Shin
Department of Mechanical and System Design Engineering, Hongik University, Seoul 121-791, Korea
(Received 29 December 2015; revised manuscript received 29 March 2016; published 24 June 2016)

We report on the numerical and theoretical study of the subcritical bifurcation of parametrically amplified waves appearing at the interface between two immiscible incompressible fluids when the layer of the lower fluid is very shallow. As a critical control parameter is surpassed, small amplitude surface waves bifurcate subcritically toward highly nonlinear ones with twice their amplitude. We relate this hysteresis with the change of shear stress using a simple stress balance, in agreement with numerical results.

DOI: 10.1103/PhysRevE.93.063114

The Faraday experiment [1] is a paradigmatic example in pattern-forming systems, due to its simplicity and richness. Standing waves appear at the interface between two fluids as they are vibrated vertically with a certain amplitude larger than a threshold at a given frequency. Extended Faraday waves have been observed with various types of fluids [2–5] on a wide range of physical configurations [6–10], displaying numerous shapes [11–14]. Localized structures have also been observed in the Faraday experiment in several situations [15–21]. The description of the nature, origin, and dynamical properties of Faraday waves has been the focus of a large scientific endeavor since the seminal work of Faraday. A particular property of these waves is their ability to display coexistence (bistability) between different wave states. Several attempts have been made to describe this feature, either from first principles [22–25] or phenomenological standpoints (see Ref. [26] and references therein), although with little or no real connection to a dynamical or structural change of the wave pattern.

In this paper, we report on the numerical simulation of hysteretic Faraday waves at the interface between two immiscible and incompressible fluids, where the lower fluid layer is very shallow. Two branches of Faraday waves are observed with different amplitudes and shapes characterized by the surface deformation and velocity field of both fluids. We propose that this hysteretic jump is related to a sudden shift in the localization of the viscous boundary layer, which moves from the interface to the bottom of the cell. We explain physically the observed hysteresis by a balance of the stresses exerted to the lower fluid layer.

We simulate numerically the equations governing the motion of two incompressible and immiscible fluids, separated by a sharp interface, using a single fluid formulation,

$$\rho\frac{D\mathbf{u}}{Dt} = -\nabla p + \rho\mathbf{G} + \nabla\cdot\mu(\nabla\mathbf{u} + \nabla\mathbf{u}^{\mathrm{T}}) + \mathbf{F}, \qquad (1)$$

where $\mathbf{u}$ is the velocity field satisfying $\nabla\cdot\mathbf{u} = 0$, $D/Dt = (\partial_t + \mathbf{u}\cdot\nabla)$ is the material derivative, and p is the pressure. The density ρ and dynamic viscosity μ remain constant within each phase. $\mathbf{F}$ and $\rho\mathbf{G}$ stand for the densities of surface tension forces located at the interface and of volume forces, respectively. Here $(\cdot)^T$ denotes the transposition operator. In the frame of reference of the vibrating fluids, $\mathbf{G} = -[g + a\cos(\omega t)]\mathbf{e}_z$, where g is gravity, a the gravity modulation amplitude, and $\omega = 2\pi/T = 2\pi f$ its angular frequency. The vector $\mathbf{e}_z$ is oriented vertically and points upwards. The force density $\mathbf{F} = \sigma\mathcal{K}\nabla I$ depends on the surface tension coefficient σ, which remains constant over the interface, the interface mean curvature $\mathcal{K}$, and an indicator function $I(x,y,z,t)$ that takes the value 0 in the heavier phase and 1 otherwise.

The problem is treated using a massively parallel numerical code explained in Refs. [27–30] that can simulate Faraday waves in big domains [31]. The simulated domain has a height $H = 10$ mm. The thickness of the lower fluid layer is $h = 1.6$ mm. The physical parameters are taken from Ref. [32]. The heavy fluid has density $\rho_1 = 1346$ kg/m^3 and dynamic viscosity $\mu_1 = 7.2\times10^{-3}$ Pa s, while for the lighter fluid $\rho_2 = 949$ kg/m^3 and $\mu_2 = 2.0\times10^{-2}$ Pa s. The surface tension is $\sigma = 35$ mN/m. The modulation frequency f is 12 Hz and its amplitude a is varied. $\mathbf{u}$ is subjected to no-slip boundary conditions at the top and bottom walls of the domain and is horizontally periodic.

The linear analysis [33] shows that using the above parameters the critical wavelength is $\lambda_c = 13.2$ mm and the critical amplitude is $a_c = 25.8$ m/s^2. The dimensions of the box in the system of coordinates (x,y,z) are $L\times W\times H = 39.6\times3.30\times10$ mm^3. The domain contains exactly three critical wavelengths longitudinally in order to spot eventual large-scale effects at high a. The y transverse dimension of the domain is small enough for the flow to remain essentially two-dimensional in the x-z plane, which we have checked numerically. The numerical resolution used in our simulation runs is $128\times8\times128$. We have checked that the same phenomena are observed with higher resolutions. Numerical stability and accuracy are assured using a dynamically bounded time step Δt [31]. To simplify our analysis, we restrict ourselves to the two-dimensional dynamics of surface waves described by the

*nperinet@ing.uchile.cl

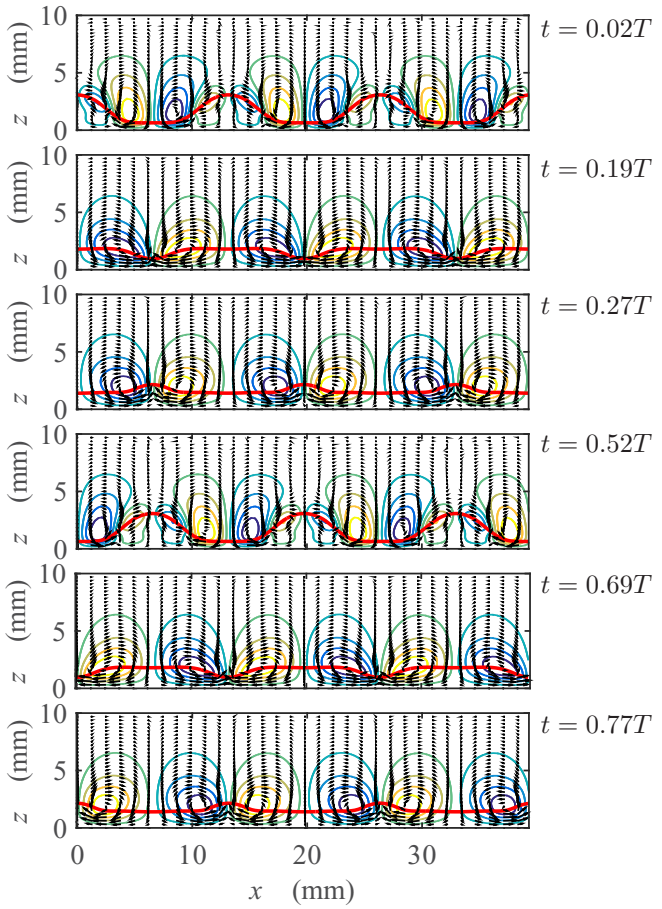

FIG. 1. Temporal snapshots of the interface deformation $\zeta(x,t)$ (thick line), velocity field $\mathbf{u}(x,z,t)$ (arrows), and stream function (contour lines) at $a = 39.5$ m/s^2 (lower branch).

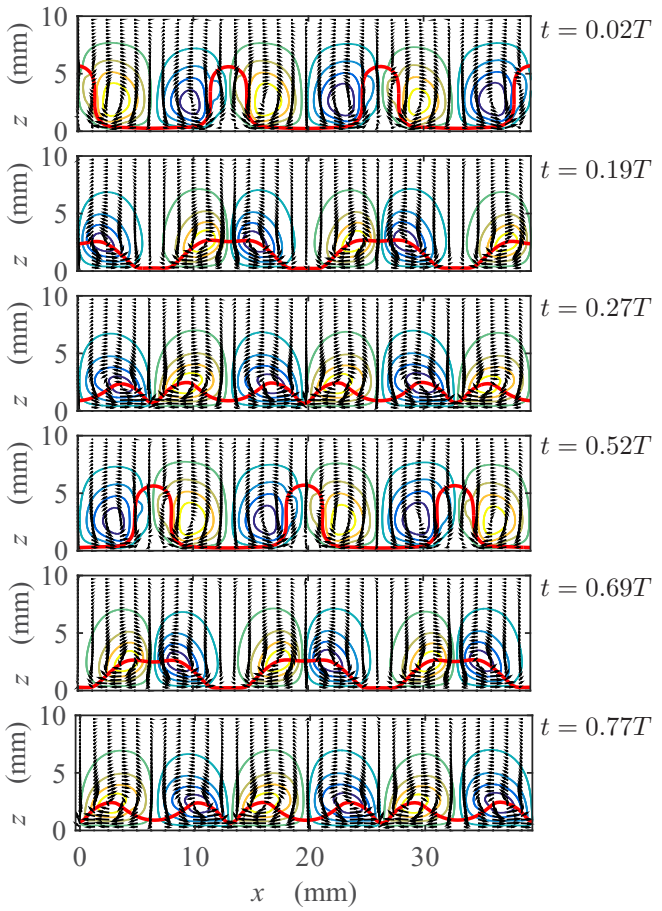

FIG. 2. Same snapshots as described in the caption of Fig. 1 at $a = 39.5$ m/s^2 (upper branch).

interface deformation $\zeta(x,t)$ and velocity field $\mathbf{u}(x,z,t)$ (as shown in Figs. 1 and 2) [34].

When a surpasses the critical value $a_c^p = 26$ m/s^2, the flat surface becomes unstable to infinitesimally small perturbations and stationary subharmonic surface gravity waves appear with a wavelength $\lambda_c = L/3$. Following Ref. [27], we show the bifurcation diagram of the saturated surface wave peak-to-peak amplitude $\Delta\zeta$ in Fig. 3(a). $\Delta\zeta$ shows the same distinctive features as the Fourier mode amplitude at λ_c and is straightforward to measure. Its dependence on a can be accurately fitted using the reduced control parameter $\epsilon = (a - a_c^p)/a_c^p$ as $\Delta\zeta \sim \epsilon^{1/2}$ for $\epsilon < 0.6$. As we increase a further than 40 m/s^2 the dependence of $\Delta\zeta$ on ϵ changes and a slight curvature toward larger values of $\Delta\zeta$ appears on the bifurcation diagram. As a exceeds $a_c^u = 41.25$ m/s^2 a secondary instability occurs: $\Delta\zeta$ increases by a factor 2 and the shape of $\zeta(x,t)$ becomes highly nonlinear, displaying localized peaks and almost horizontal troughs of constant length $l_F \simeq 8$ mm. The thickness of these troughs at a_c^u in the upper branch of the bifurcation, $h_F \simeq 0.25$ mm, is twice as small as the one on the lower branch, as depicted in Fig. 3(b). These variables are defined geometrically in Fig. 3(c). As a consequence of mass conservation while $\Delta\zeta$ becomes larger h_F becomes smaller. In the upper branch $\zeta(x,t)$ also becomes multivalued. To avoid misinterpretations of the bifurcation diagram by following $\Delta\zeta$ as $\zeta(x,t)$ becomes multivalued in the upper branch, we have also used the angle $\theta(s)$ that the local tangent to the interface makes with the x axis at normalized arc length s as an order parameter [see Fig. 3(c)]. $\theta(s)$ is single valued for all values of a. We have computed the Fourier amplitude at λ_c of $\theta(s)$ in arc length s, $\hat{\theta}$, which displays the same bifurcation diagram as $\Delta\zeta$ [see Fig. 3(a)]. A hysteresis loop is displayed as this state is sustained decreasing a until $a_c^d = 39.25$ m/s$^2 \neq a_c^u$ [see Fig. 3(a)]. To wit, we show in both Figs. 1(a) and 1(b) $\zeta(x,t)$ and $\mathbf{u}(x,z,t)$ for the same value of $a = 39.5$ m/s^2.

Hysteresis is also reflected in the changes of the velocity field properties, specifically, how the energy dissipation rate $\tau(\mathbf{u}) = \mu \sum_{i,j=1}^{2} (\partial \mathbf{u}_i/\partial x_j)^2$ evolves as a increases. We first focus on the mean dissipation rate $\langle \tau(\mathbf{u}) \rangle$. Here $\langle \cdot \rangle$ stands for time average. The amplitude jump and hysteresis loop observed for $\Delta\zeta$ and $\hat{\theta}$ are also observed for the space-averaged mean dissipation rate $\frac{1}{V}\int_V \langle \tau(\mathbf{u}) \rangle dV$ as shown in Fig. 4(a). A roughly linear dependence on a can be observed, with different slopes for lower and upper branches. A spatial change in the structure of τ can be also observed by measuring the dissipation rate of the mean velocity $\tau(\langle \mathbf{u} \rangle)$. For the lower branch, the largest values of $\tau(\langle \mathbf{u} \rangle)$ are localized at the interface where the shearing of both fluids is the strongest. The profile of $\tau(\langle \mathbf{u} \rangle)$ changes in the upper branch: $\tau(\langle \mathbf{u} \rangle)$ presents maxima

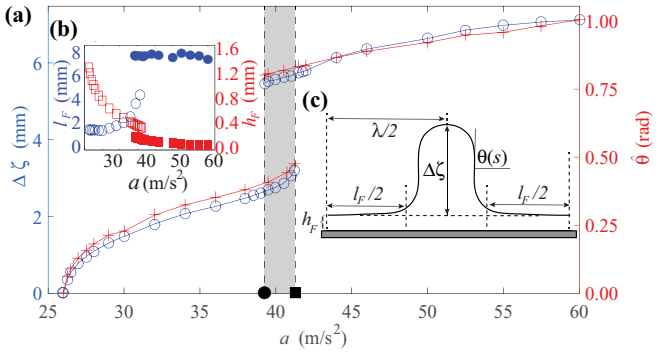

FIG. 3. (a) Bifurcation diagram for $\Delta\zeta$ (○) and $\hat{\theta}$ (+) as a function of a for the weakly (lower branch) and highly (upper branch) nonlinear saturated wave. Hysteresis occurs in the shaded region: $a_c^d = 39.25$ m/s^2 (●) and $a_c^u = 41.25$ m/s^2 (■) are displayed in the acceleration axis. (b) l_F (○) and h_F (□) as a function of a on the lower (open symbols) and upper (full symbols) branches of the bifurcation diagram. (c) Surface deformation $\zeta(x,t)$ (continuous line) at $a = 39.5$ m/s^2 showing the definition of $\theta(s)$ and $\Delta\zeta$ for the upper branch of the bifurcation diagram.

at the interface and also at the bottom of the domain. When a is further increased, $\tau(\langle\mathbf{u}\rangle)$ becomes localized at the bottom of the cell where the viscous boundary layer dissipates the largest part of the kinetic energy of the flow. The difference in structure of $\tau(\langle\mathbf{u}\rangle)$ for $a = 39.5$ m/s^2 is shown in Figs. 4(b) and 4(c). All temporal Fourier components of τ display the same bifurcation diagram as $\langle\tau(\mathbf{u})\rangle$ (not plotted here), showing that the structural change is a global one.

To explain this hysteretic transition and the qualitative changes reported above at the transition we present a physical explanation relating the above data. We propose that the amplitude jump and wave hysteresis can be understood from a balance between lubrication and hydrostatic stresses [21,35] that is coupled with a change of the flow regime within the film.

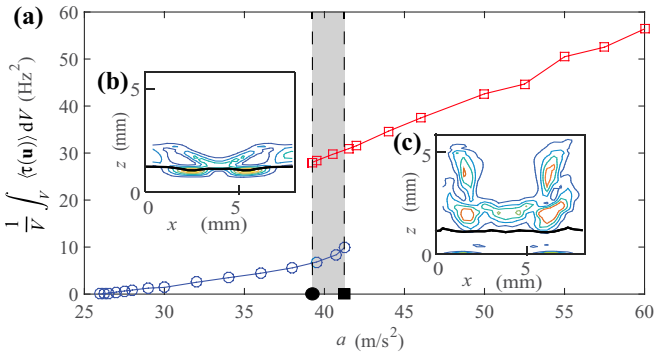

FIG. 4. (a) Bifurcation diagram for the space-averaged dissipation rate of the mean velocity $\frac{1}{V}\int_V\langle\tau(\mathbf{u})\rangle$ as a function of a for the weakly (○) and highly (□) nonlinear saturated wave. Hysteresis occurs in the shaded region: $a_c^d = 39.25$ m/s^2 (●) and $a_c^u = 41.25$ m/s^2 (■) are displayed in the acceleration axis. Insets: Contour lines of $\tau(\langle\mathbf{u}\rangle)$ for $a = 39.5$ m/s^2 in the lower (b) and upper (c) branches. The brighter the lines, the higher the dissipation. The thick dark line is the interface.

From the data displayed in Fig. 3(a), the depth of the layer reduces to $h_F = h - \Delta\zeta/2 \simeq 0.5$ mm at a_c^u on the lower branch of the bifurcation, occurring roughly over $\lambda_c/2$ (see Figs. 1 and 3(c)). At this point the Reynolds number $\mathrm{Re}^u = \rho_1\omega h_F^2/\mu_1 \simeq 4$ and a transition occurs as the viscous stress within the film increases, forcing the hydrostatic stress to do the same. Then, a new equilibrium state is reached in the upper branch, with a thinner h_F and a larger l_F [see Figs. 2 and 3(b)]. In this upper branch, the flow in the thin film is described by Stokes dynamics $\nabla p = \mu_1\nabla^2\mathbf{u}$, assuming that $\partial_z \gg \partial_x, u \gg w$, and p is constant along the z direction, where u, w, and p stand for the horizontal and vertical components of the velocity $\mathbf{u}$ and the pressure, respectively. Hence

$$\partial_{zz}u = \frac{\Delta p}{\mu_1 l_F}, \quad \nabla^2 w = 0, \tag{2}$$

where Δp is the difference between the pressure in the lower fluid under the column and inside the film. Assuming zero velocity at the bottom of the domain $z = 0$ and a stress-free interface $\partial_z u = 0$ at $z = h_F$, the solution of Eq. (2) is

$$u = \frac{\Delta p}{\mu_1 l_F}\left(\frac{z^2}{2} - h_F z\right), \tag{3}$$

which is averaged over the fluid height to evaluate the viscous stress $\sigma_s = 3\mu_1 l_F\bar{u}/h_F^2$. This stress makes the film resist detaching when a viscous regime is achieved at $\mathrm{Re} = \rho_1\omega h_F^2/\mu_1 < \mathrm{Re}^d \simeq 1$. The critical Reynolds number Re^d is calculated for h_F at the transition from the upper to the lower branch in Fig. 3(a) and it sets a critical depth $h_0 \sim 0.25$ mm. From dimensional analysis, one expects $\bar{u} \sim \omega l_F$, which is confirmed by our numerical simulations as $\bar{u}/\omega l_F \simeq 1/12$ in the upper branch. Hence, $\sigma_s \simeq \mu_1 l_F^2\omega/(4h_F^2)$ and the force per unit length arising from this shear stress, $F_s \simeq \mu_1\omega l_F^3/(12h_F^2)$, must compensate the hydrostatic pressure contribution F_h from both ends of the film at maximum acceleration, to ensure the film sustainment. The stress balance reads $F_s = 2F_h$, where F_h is given at each border of the film by the difference of hydrostatic pressure between the zone inside the film and the zone outside the film: $F_h \simeq (\rho_1 - \rho_2)(a^* + g)\Delta\zeta^2$, a^* denoting the maximum acceleration. After the transition, F_s and F_h are estimated at 300 mN/m in the upper branch, which is 10 times larger than the stress contribution from surface tension that is consequently neglected. Using mass conservation $h\lambda_c \simeq \Delta\zeta(\lambda_c - l_F)$ to relate $\Delta\zeta$, h_F, and l_F, the balance reads,

$$l_F^3(\lambda_c - l_F)^2 \simeq \frac{6gh^2\lambda_c^2\mathrm{Re}}{\omega^2}\left(1 + \frac{a^*}{g}\right)\left(1 - \frac{\rho_2}{\rho_1}\right), \tag{4}$$

where $\mathrm{Re} < \mathrm{Re}^d$, according to our simulation results on the upper branch (lubrication flow) and ω is given by the dispersion relation for shallow waves,

$$\omega^2 = \left(\frac{\rho_1 - \rho_2}{\rho_1 + \rho_2}\right)\frac{16\pi^2}{\lambda_c^2}gh, \tag{5}$$

with the forcing frequency ω is twice that of the fluid's response. At $\mathrm{Re} = \mathrm{Re}^d$, the stress balance takes the form

$$l_F^3(\lambda_c - l_F)^2 \simeq \frac{3h\lambda_c^4}{8\pi^2}\left(1 + \frac{a^*}{g}\right)\left(1 + \frac{\rho_2}{\rho_1}\right). \tag{6}$$

The left-hand side of this balance reaches its maximum when $l_F = 3\lambda_c/5 \simeq 7.9$ mm, close to the constant value found in our simulations for l_F in the upper branch. Thus, $\Delta\zeta \simeq 5$ mm and the stress balance is achieved when $a^*/g \simeq 3.4$. As l_F rests constant in the upper branch, when $a > a^*$, h_F decreases to compensate the increase in F_h. When $a < a^*$, $h_F > h_0$ (Re > 1), changing the nature of the flow from lubrication ($\sigma_s \sim l_F^2/h_F^2$) to viscous flow ($\sigma_s \sim l_F/h_F$). With this functional change F_s cannot sustain F_h, as it is $l_F/h_F \sim 30$ times smaller. We conjecture that this shift in magnitude for σ_s as the film changes its thickness is the reason for the observed amplitude jump.

In summary, using numerical simulations, we have observed the hysteretic bifurcation of Faraday waves in very shallow layers. The coexistence between weakly and highly nonlinear Faraday waves, observed experimentally, is now confirmed numerically and understood as the bifurcation of a wave pattern presenting hysteresis, which we conjecture is related to the structural shift of the viscous shear rate. The loop mechanism can be understood by stress balance between hydrostatic and shear stresses, which changes as the depth of the layer becomes shallower than the boundary layer of the fluid. This simple treatment is a first approach toward a more profound understanding of patten selection where dynamic changes in dissipation or structure are present, and it opens questions related to the nature and origin of the hysteresis loop in shallow layers of Newtonian and complex fluids. In that context, the proposition of a phenomenological model away from the weakly nonlinear limit would be a natural continuation of this work that can potentially explain complex bifurcations of highly nonlinear Faraday waves [36].

We thank L. Tuckerman and M. G. Clerc for fruitful discussions and acknowledge the financial support of FONDECYT Grants No. 1130354 and No. 3140522 as well as the Basic Science Research Program through the National Research Foundation of Korea (NRF) funded by the Ministry of Science, ICT and future planning (Grant No. NRF-2014R1A2A1A11051346). This research was supported by the supercomputing infrastructure of the NLHPC (ECM-02) and GENCI (IDRIS).

[1] M. Faraday, Philos. Trans. R. Soc. London **121**, 299 (1831).
[2] C. Wagner, H. W. Müller, and K. Knorr, Phys. Rev. Lett. **83**, 308 (1999).
[3] F. Raynal, S. Kumar, and S. Fauve, Eur. Phys. J. B **9**, 175 (1999).
[4] I. Aranson and L. Tsimring, Rev. Mod. Phys. **78**, 641 (2006).
[5] P. Ballesta and S. Manneville, J. Non-Newtonian Fluid Mech. **147**, 23 (2007).
[6] S. Fauve, S. Douady, and O. Thual, J. Phys. II **1**, 311 (1991).
[7] R. G. Holt and E. H. Trinh, Phys. Rev. Lett. **77**, 1274 (1996).
[8] A. Kudrolli, M. C. Abraham, and J. P. Gollub, Phys. Rev. E **63**, 026208 (2001).
[9] C. Falcón, U. Bortolozzo, E. Falcon, and S. Fauve, Europhys. Lett. **86**, 14002 (2009).
[10] G. Pucci, E. Fort, M. Ben Amar, and Y. Couder, Phys. Rev. Lett. **106**, 024503 (2011).
[11] B. Christiansen, P. Alstrøm, and M. T. Levinsen, Phys. Rev. Lett. **68**, 2157 (1992).
[12] W. S. Edwards and S. Fauve, Phys. Rev. E **47**, R788 (1993).
[13] A. Kudrolli, B. Pier, and J. P. Gollub, Physica D **123**, 99 (1998).
[14] A. M. Rucklidge, M. Silber, and A. C. Skeldon, Phys. Rev. Lett. **108**, 074504 (2012).
[15] J. Wu, R. Keolian, and I. Rudnick, Phys. Rev. Lett. **52**, 1421 (1984).
[16] P. B. Umbanhowar, F. Melo, and H. L. Swinney, Nature **382**793 (1996).
[17] F. S. Merkt, R. D. Deegan, D. I. Goldman, E. C. Rericha, and H. L. Swinney, Phys. Rev. Lett. **92**, 184501 (2004).
[18] O. Lioubashevski, Y. Hamiel, A. Agnon, Z. Reches, and J. Fineberg, Phys. Rev. Lett. **83**, 3190 (1999).
[19] H. Arbell and J. Fineberg, Phys. Rev. Lett. **85**, 756 (2000).
[20] J. Rajchenbach, A. Leroux, and D. Clamond, Phys. Rev. Lett. **107**, 024502 (2011).
[21] C. Falcón, J. Bruggeman, M. Pasquali, and R. D. Deegan, Europhys. Lett. **98**, 30006 (2012).
[22] P. Chen and J. Viñals, Phys. Rev. Lett. **79**, 2670 (1997).
[23] W. Zhang and J. Viñals, J. Fluid Mech. **336**, 301 (1997).
[24] A. C. Skeldon and G. Guidoboni, SIAM J. Appl. Math. **671**064 (2007).
[25] A. C. Skeldon and A. M. Rucklidge, J. Fluid Mech. **777**, 604 (2015).
[26] M. C. Cross and P. C. Hohenberg, Rev. Mod. Phys. **65**, 851 (1993).
[27] N. Périnet, D. Juric, and L. S. Tuckerman, J. Fluid Mech. **635**, 1 (2009).
[28] S. Shin, J. Comput. Phys. **222**, 872 (2007).
[29] S. Shin and D. Juric, Int. J. Num. Meth. Fluids **60**, 753 (2009).
[30] S. Shin, J. Chergui, and D. Juric, arXiv:1410.8568 [physics.flu-dyn].
[31] L. Kahouadji, N. Périnet, L. S. Tuckerman, S. Shin, J. Chergui, and D. Juric, J. Fluid Mech. **772**, R2 (2015).
[32] A. V. Kityk, J. Embs, V. V. Mekhonoshin, and C. Wagner, Phys. Rev. E **72**, 036209 (2005); **79**, 029902(E) (2009).
[33] K. Kumar and L. S. Tuckerman, J. Fluid Mech. **279**, 49 (1994).
[34] See Supplemental Material at http://link.aps.org/supplemental/10.1103/PhysRevE.93.063114 for the dynamics of the hysteretic Faraday waves.
[35] H. Ockendon and J. R. Ockendon, *Viscous Flow* (Cambridge University Press, New York, 1995).
[36] U. Bortolozzo, M. G. Clerc, C. Falcón, S. Residori, and R. Rojas, Phys. Rev. Lett. **96**, 214501 (2006).